AGU PUBLICATIONS

JGR

Journal of Geophysical Research: Planets

RESEARCH ARTICLE
10.1002/2013JE004556

Special Section:
Results from the first 360 Sols of the Mars Science Laboratory Mission: Bradbury Landing through Yellowknife Bay

Key Points:
- DAN special campaign in Yellowknife Bay
- DAN local measurements of water and chlorine abundance
- Correlation of DAN measurements and geological context

Correspondence to:
M. L. Litvak,
litvak@mx.iki.rssi.ru

Citation:
Litvak, M. L. et al. (2014), Local variations of bulk hydrogen and chlorine-equivalent neutron absorption content measured at the contact between the Sheepbed and Gillespie Lake units in Yellowknife Bay, Gale Crater, using the DAN instrument onboard Curiosity, *J. Geophys. Res. Planets*, *119*, 1259–1275, doi:10.1002/2013JE004556.

Received 10 OCT 2013
Accepted 15 MAY 2014
Accepted article online 22 MAY 2014
Published online 13 JUN 2014

Local variations of bulk hydrogen and chlorine-equivalent neutron absorption content measured at the contact between the Sheepbed and Gillespie Lake units in Yellowknife Bay, Gale Crater, using the DAN instrument onboard Curiosity

M. L. Litvak[1], I. G. Mitrofanov[1], A. B. Sanin[1], D. Lisov[1], A. Behar[2], W. V. Boynton[3], L. Deflores[2], F. Fedosov[1], D. Golovin[1], C. Hardgrove[4], K. Harshman[3], I. Jun[2], A. S. Kozyrev[1], R. O. Kuzmin[1,5], A. Malakhov[1], R. Milliken[6], M. Mischna[2], J. Moersch[4], M. Mokrousov[1], S. Nikiforov[1], V. N. Shvetsov[7], K. Stack[8], R. Starr[9], C. Tate[4], V. I. Tret'yakov[1], A. Vostrukhin[1], and the MSL Team

[1]Space Research Institute—RAS, Moscow, Russia, [2]Jet Propulsion Laboratory, Pasadena, California, USA, [3]University of Arizona, Tucson, Arizona, USA, [4]University of Tennessee, Knoxville, Tennessee, USA, [5]Vernadsky Institute for Geochemistry and Analytical Chemistry, Moscow, Russia, [6]Brown University, Providence, Rhode Island, USA, [7]Joint Institute for Nuclear Research, Dubna, Russia, [8]California Institute of Technology, Pasadena, California, United States, [9]Catholic University of America, Washington D. C., Washington, USA

Abstract Data gathered with the Dynamic Albedo of Neutron (DAN) instrument onboard rover Curiosity were analyzed for variations in subsurface neutron flux and tested for possible correlation with local geological context. A special DAN observation campaign was executed, in which 18 adjacent DAN active measurements were acquired every 0.75–1.0 m to search for the variations of subsurface hydrogen content along a 15 m traverse across geologic contacts between the Sheepbed and Gillespie Lake members of the Yellowknife Bay formation. It was found that several subunits in Sheepbed and Gillespie Lake could be characterized with different depth distributions of water-equivalent hydrogen (WEH) and different chlorine-equivalent abundance responsible for the distribution of neutron absorption elements. The variations of the average WEH at the top 60 cm of the subsurface are estimated at up to 2–3%. Chlorine-equivalent neutron absorption abundances ranged within 0.8–1.5%. The largest difference in WEH and chlorine-equivalent neutron absorption distribution is found between Sheepbed and Gillespie Lake.

1. Introduction

Observations performed by various missions over the past decade have revealed a complex mineralogical and aqueous history of Mars, which could be associated with habitable environments [see, for example, *Squyres et al.*, 2004, 2012; *Bibring et al.*, 2006; *Grotzinger*, 2009; *Murchie et al.*, 2009]. The Mars Science Laboratory (MSL) rover Curiosity has been specially developed to determine whether Mars could ever have had habitable environment. To do this, the MSL rover was equipped with 11 different science instruments, which were selected to provide joint in situ studies [*Grotzinger et al.*, 2012].

Gale Crater was chosen as the MSL landing site, because orbital observations revealed the presence of ancient, multilayered deposits of various hydrated minerals (clays and sulfates) on the flanks of the central uplift (now known as Mount Sharp), which could be assessed by a rover [*Golombek et al.*, 2012; *Grotzinger et al.*, 2012]. The geology of Gale Crater is characterized by a mixture of alluvial fan, high thermal inertia/high-albedo stratified deposits, and a number of stratigraphically/geomorphically distinct fluvial features [*Grotzinger et al.*, 2012].

In situ analysis accomplished within several weeks after landing has shown that there are geological targets of high scientific value in the vicinity of the landing site. One of them is a triple junction point located at the Yellowknife Bay formation within 450 m of the landing site, distal to the toe of the Peace Vallis alluvial fan [*Grotzinger et al.*, 2013; *Vaniman et al.*, 2013]. This area presents a combination of several geological units with different thermal inertia, stratified rocks, and the presence of clay and sulfate minerals. The decision was made to traverse eastward and downhill, as close as possible to the triple junction, to make the MSL's first analysis of a drilled sample [*Grotzinger et al.*, 2013]. This approach resulted in an ~750 m traverse (measured in

wheel odometry). Curiosity successfully accomplished sampling operations (see *Anderson et al.* [2012] for details of the MSL sample acquisition system) of the aeolian deposits named Rocknest and the mudstones located at the lowest part of the Yellowknife Bay formation [*Bish et al.*, 2013; *Blake et al.*, 2013; *Leshin et al.*, 2013; *Meslin et al.*, 2013; *Grotzinger et al.*, 2013; *Ming et al.*, 2013; *Vaniman et al.*, 2013].

Here we focus on one aspect of Curiosity's observations in Yellowknife Bay related to the monitoring of local variations in subsurface hydrogen/neutron absorption distributions using an active neutron spectroscopy. We have analyzed data gathered by the Dynamic Albedo of Neutron (DAN) instrument installed on board the rover Curiosity. DAN was selected for the mission to provide the monitoring of the distribution of hydrogen-rich material (primarily physically adsorbed water and bound water in hydrated minerals) in the Martian subsurface along Curiosity's traverse [*Litvak et al.*, 2008; *Mitrofanov et al.*, 2012, 2013a, 2013b].

Our analysis employs the technique for the estimation of the water-equivalent hydrogen (WEH) from the DAN active neutron spectrometry data (see overview of data reduction procedures in section 3). *Mitrofanov et al.*, [2013a, 2013b] have used this method to estimate the WEH abundances at each location along Curiosity's traverse from Bradbury Landing to the Yellowknife Bay formation and along the first portion of the traverse to the foot of Mount Sharp (it covers the first year of operations on the Martian surface). Normally, DAN active observations are performed each time the rover concludes a Martian solar day (sol)'s drive and sometimes at stops in the middle of a drive. During the first 360 sols of the mission, Curiosity covered ~1850 m with 190 active measurements made at intervals of ~20–40 m [*Mitrofanov et al.*, 2013b].

The data analysis presented in this paper includes a small part of rover's route across different geological units inside the Yellowknife Bay formation, starting from the drilling sites known as John Klein and Cumberland and continuing up to the Gillespie Lake member of the Yellowknife Bay formation. These measurements were accomplished within a special DAN observation campaign to test the potential variability of hydrogen on a small horizontal scale, comparable with the DAN footprint, and determine whether it is correlated with local variations in geology that were observed by the other MSL instruments. Within the DAN observation campaign discussed here, the rover covered a short traverse of just ~15 m, but with 18 active measurements made at intervals of only 0.75–1 m. The path for this traverse was chosen to cross the different geological subunits inside the Yellowknife Bay formation, with a ground track approximately perpendicular to the geologic contacts.

The measurement strategies for this DAN observation campaign are presented in section 4. Section 5 describes the results from the DAN measurements along the traverse through the Sheepbed/Gillespie Lake contact area and the correlation with geological context. For background, we have also added short descriptions of the DAN instrument (section 2) and an overview of the data reduction and model depended deconvolution procedures (section 3), which are also discussed by *Mitrofanov et al.*, 2013b.

2. DAN Instrument

The Dynamic Albedo of Neutron (DAN) instrument on MSL [*Litvak et al.*, 2008; *Mitrofanov et al.*, 2012] was designed to measure the hydrogen content of the regolith to a depth of approximately 60 cm. The instrument is located at the back of the rover together with the Multi-Mission Radioisotope Thermoelectric Generator (MMRTG). DAN consists of two separate blocks integrated onto the two sides of the rover: a pulsed neutron generator (DAN/PNG) and a detector element (DAN/DE). DAN may be operated both in active and in passive modes of measurements. In active mode, the DAN/PNG produces 2 μs pulses of high-energy (14.1 MeV) neutrons (10^7 neutrons per pulse) emitted in 4π around the DAN/PNG. A significant fraction of these neutrons penetrate into the subsurface under the rover and interact with soil nuclei. The neutrons lose energy through inelastic scattering reactions with nuclei in the subsurface. Some of the moderated neutrons leak back out of the subsurface where they are counted by the DAN/DE subsystem as a function of time after the neutron pulse.

The DAN/DE consists of two proportional counters filled with ^{3}He gas at a pressure of three atmospheres. The ^{3}He nucleus has a large cross section for capture of low-energy neutrons in the reaction $n + {}^3\mathrm{He} \rightarrow {}^3\mathrm{H} + p + 764$ keV. The released energy of the reaction is distributed between a triton ^{3}H and a proton with 191 keV and 573 keV energies, respectively, in inverse proportion to their masses. The shape of pulse height spectrum measured in ^{3}He detector does not depend on the energy of

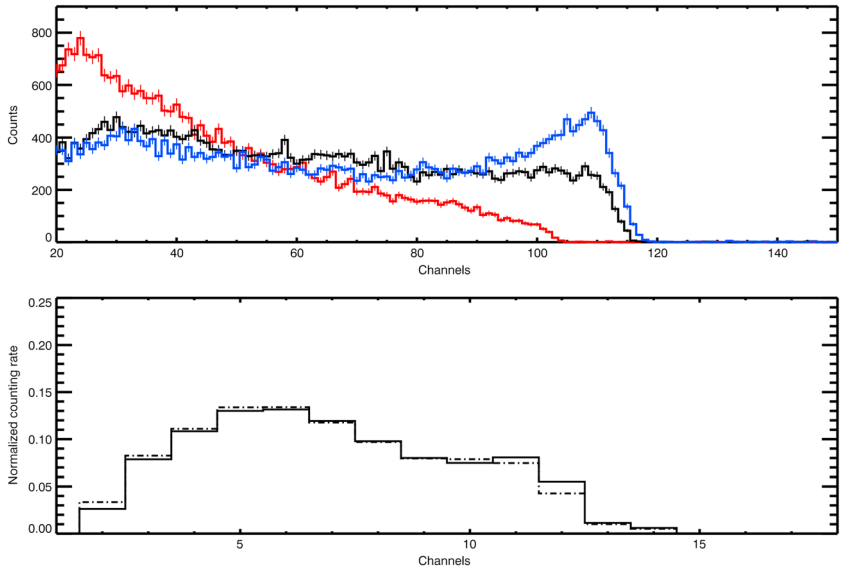

Figure 1. (top) The pulse height spectra measured in ground tests with DAN proportional counters with different amplifier time constants equal to 1 μs (red), 3 μs (black), and 6 μs (blue). (bottom) The examples of 16-channel pulse height spectra measured by the DAN/DE flight unit onboard MSL rover Curiosity at the beginning of the surface operation (dash-dot line) and at the end of the MSL primary mission (solid line).

incident neutron but depends on the kinematic of the reaction process and selection of amplifier time constant [see, for example, *Crane and Baker*, 1991]. The typical shape of the spectrum has a main peak, which corresponds to the maximum energy deposited in the detector if both the proton and the triton are stopped in the detector's volume (764 keV). The other cases when proton or triton reaches detector's wall produce low-energy tail in the spectrum (not all released energy is deposited in the detector volume). The selection of amplifier time constant can significantly change the typical shape of the spectrum because it determines the degree of charge collection in the detector. Large values of the amplifier time constant provide complete charge collection and produce the shape of the pulse height spectrum with a distinct peak at 764 keV as described above. Vice versa, too short-time constant causes complete loss of the primary peak but decreases dead time of the detector system and allows to achieve more higher counting rates [see, for example, *Crane and Baker*, 1991]. As a preparation to DAN active measurements (requirement to detect high counting rate in time bins following PNG neutron pulse), we have tried to find a compromise between good resolution of pulse height spectrum and ability to detect higher counting rates. We have performed a set of ground tests with DAN proportional counters using different amplifier time constants. On Figure 1 (top), we have illustrated the results of these tests by showing spectra measured for time constant equal to 1 μs (red), 3 μs (black), and 6 μs (blue). The optimal spectra resolution and classic shape of pulse height spectrum is achieved at 6 μs time constant (blue), 1 μs time corresponds to full loss of total deposition peak, and 3 μs causes intermediate results. The last case was considered as a base option (final value of time constant was selected as 2.5 μs) to get reasonable compromise between requirements to keep more or less the shape of the spectrum and to provide the detection of higher counting rate. Final digitization of the pulse height spectrum in DAN flight model was done as linear 16 channels. It is enough to represent selected shape of the pulse height spectrum and monitor it during surface operations. On Figure 1 (bottom), we have shown two DAN spectra measured at the beginning of the surface operation (right after landing) and at the end of the primary mission (>1.5 years later) to illustrate both the shape of the DAN pulse height spectrum and its stability with time.

The first DAN/DE proportional counter is wrapped in a lead enclosure (to protect detector from X-rays generated by the DAN/PNG) and is sensitive to thermal neutrons and epithermal neutrons with energies up to 1 keV (detection efficiency drops more than 100 times for the neutrons at such energies) [see *Mitrofanov et al.*, 2012, Figure 6]. The second proportional counter is wrapped in a cadmium enclosure with a thickness of about

1 mm. It helps to cut off X-rays from the DAN/PNG, but specifically, it is done to absorb thermal neutrons. The difference in counting rates between the two detectors provides an estimation of the counting rate associated with thermal neutrons.

The counts in the detectors are recorded as a function of time after each DAN/PNG neutron pulse. This time history of neutrons that have scattered in the subsurface is known as a "die-away" curve. The total duration of a die-away curve lasts from tens of microseconds (for epithermal neutrons) up to hundreds of microseconds (for the thermal neutrons) after each pulse. Typically, the die-away curves from thousands of individual pulses in a single location are coadded to improve counting statistics. The duration, shape, and amplitude of die-away curves provide information about the time history of the moderation of fast neutrons and strongly depend on the subsurface structure and distribution of hydrogen (the most efficient moderation element). Other elements in the subsurface also influence die-away curves. In particular, the presence of elements with high thermal neutron absorption cross sections can depress the population of thermal neutrons that leak out of the surface [*Hardgrove et al.*, 2011, 2013]. Several elements (for example, Cl, Fe, Ti, Mn, and Gd) have large cross section for thermal neutron absorption. In our analysis, for simplicity, we use the content of chlorine as a variable parameter of modeling DAN data and fix abundance of other absorbing elements at the average level. It may be considering as "chlorine-equivalent" parameter for accounting of all absorbers of thermal neutrons (see also for details section 3 and *Mitrofanov et al.* [2013b]).

DAN can operate in both active (measurement of die-away curves) and passive modes. Active observations provide many details about the distribution of hydrogen, but they are resource intensive and limited by the DAN/PNG lifetime. In passive mode, DAN/PNG is off, and DAN/DE measures only the neutron radiation background produced by the MMRTG and galactic cosmic rays (GCRs). Passive measurements are complimentary to active measurements and can be used for monitoring the bulk subsurface hydrogen content during the rover's drives and continuous monitoring of radiation background while the rover is stationary. The analysis of passive observations is not the goal of the paper, but some details are presented by *Jun et al.* [2013a, 2013b] and *Tate et al.* [2013]. Passive mode observations are also very useful for making direct comparisons with orbital observations [*Litvak et al.*, 2013] to search for simultaneous background radiation variations on orbit and at the surface.

Details of DAN design, principles of operations, and main science tasks are also presented by *Litvak et al.* [2008] and *Mitrofanov et al.* [2012].

3. DAN Data Reduction Procedures

3.1. Numerical Modeling

DAN measures variations in the neutron flux from the subsurface that are affected by many factors, including hydrogen distribution, subsurface structure, the presence of neutron absorbing elements, and soil density variations. To describe the variations of neutron flux in terms of these physical parameters, most importantly in terms of water abundance, model-dependent data deconvolution must be used. In this approach, we postulate a model of the subsurface with unknown parameters and find best estimates of these parameters through the comparison of numerical prediction of neutron flux for the given model with experimental data. To implement it, one should create numerical models of DAN/DE and DAN/PNG, MSL rover structure, and Martian regolith with different distribution of water and elemental composition. In our study for the numerical modeling of neutron interactions, we have used the well known and commonly accepted Monte Carlo N-Particle eXtended (MCNPX) code developed at the Los Alamos National Laboratory [see, for example, *Pelowitz*, 2011].

The DAN/PNG was modeled as a simple point source of monoenergetic (14.1 MeV) neutrons emitted isotropically and having Gaussian type of time profile with full width at half maximum equal to ~2 μs. The DAN/DE numerical model has been created from the instrument engineering drawings. Its main part contains two ^{3}He proportional neutron detectors with three atmosphere gas pressure: counter of thermal neutrons (CTN) and counter of epithermal neutrons (CETN). For more details, efficiency curves of these detectors could be found in *Mitrofanov et al.* [2012].

The detailed information about the rover mechanical structures and chemical composition is not available, but the main properties of the rover could be adjusted from the ground tests and functional measurements

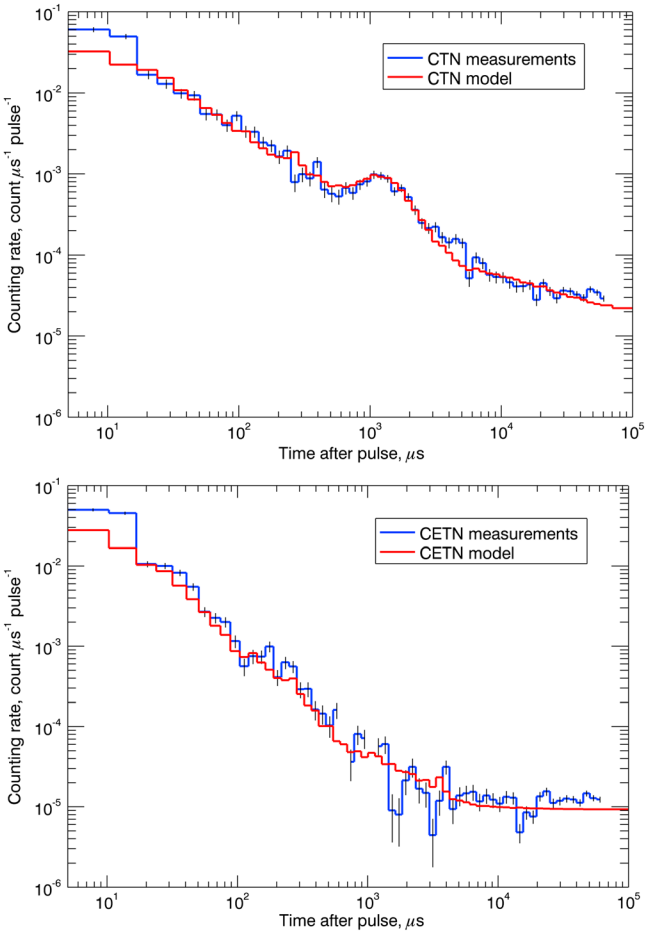

Figure 2. The measured (blue line) and numerically simulated (red line) DAN die-away time profiles for the ATLO prelaunch tests.

where DAN was integrated onboard Curiosity. Here we continue to develop a simplified model of the rover presented in *Jun et al.* [2013b] using DAN active measurements made at the MSL prelaunch tests at the Kennedy Space Center (assembly, test, and launch operations or ATLO tests). We have modeled rover position, orientation, and test environment including concrete floor, walls, and ceiling in accordance with the testing facility geometry. The model of the rover included main chassis (dimensions 120 cm × 162 cm × 44 cm), wheels, and a detailed model of the MMRTG—a nuclear power source for MSL [see for more details *Jun et al.*, 2013b]. MMRTG generates electrical power using plutonium isotopes (primarily of ^{238}Pu with half-life of 86.4 years) in the PuO_2 fuel and produces a continuous flux of neutrons with broad-energy spectrum. We have achieved reasonable statistical agreement between ATLO measured data and numerical simulations adjusting the parameters of rover model (Figure 2). Final model of the rover structure has a total mass of about 900 kg and contains uniformly distributed material with density 0.95 g/cm^3 and composition: 0.4 wt % of hydrogen, 3.2 wt % of carbon, 16.0 wt % of oxygen, 39.13 wt % of aluminum, 7.83 wt % of nitrogen, 31.30 wt % of titanium, and 2.14 wt % of copper.

The rover body may contribute additional background in DAN active measurements, because large rover mass efficiently scatters neutrons escaping from the regolith. To take the rover into account, we have modeled CTN and CETN die-away curves $F_{tn}(t)$ and $F_{etn}(t)$ with and without rover presence in our numerical model. We have tried to find convolution function $R(t)$ for each DAN detector describing difference between measurements caused with rover presence: $W_{tn,etn}(t) = F_{tn,etn}(t) \cdot R_{tn,etn}(t)$. This approach helps to save computational time during modeling of active measurements on the Martian surface and at the same time simplifies updating the rover model. When the next rover model will be available, we will change the correction factors $R(t)$ without needing to reproduce a large set of MCNPX calculations.

The Martian atmosphere for all the DAN active measurements has been modeled as a uniform gas layer with density 1.6×10^{-5} g/cm^3, temperature 213 K, and fixed composition (major elements: C, O, N, and Ar).

The average regolith composition at Gusev and Meridiani measured by the MERs [see *Bell*, 2008] has been used as our representative regolith model. In the next data reduction interaction, we plan to update it with the measurements of elemental composition performed onboard Curiosity. The common difficulties with adjustment of elemental composition for DAN data analysis are related with a significant difference in the instruments footprints. Instruments, which are providing subsurface composition, analyze only small spot on the surface or process a tiny soil sample taken from the very top of the subsurface. DAN collects information about a large volume (~1.5 m radius × ~60 cm in depth) of regolith directly below the DAN instrument.

Average properties of this regolith volume may be significantly different from a small surface spot or soil sample studied by another instruments.

The production, moderation, and loss of neutrons in the regolith depend on the amount of chemical elements with large neutron interaction cross sections. So the presence of such abundant elements as iron, chlorine, and hydrogen is important for DAN numerical modeling [see, for example, *Hardgrove et al.*, 2011]. It is necessary to analyze the presence of iron and chlorine, because it influences the shape of die-away curve and can impede the estimation of hydrogen content. The chlorine has a significantly higher cross section to capture thermal neutrons than iron [see, for example, *Hardgrove et al.*, 2011]. The Alpha-Particle X-ray Spectrometer (APXS) data show that relative variations of the chlorine from one Curiosity location to another are quite large (it could be as large as 2–3 times) [see, for example, *Gellert et al.*, 2014; *Berger et al.*, 2014]. From other side, it looks like that in many cases, iron does not show so large relative variations along the traverse [*Gellert et al.*, 2014]. That is why for simplicity, we have used the chlorine content in the form of a chlorine-equivalent parameter to account for all thermal neutron absorbing elements. That means that the content n_{equ} corresponds to the contribution of all absorbing nuclei, as

$$n_{equ} = \left(n_{Cl} + \frac{\sum_A ((n_A - n_{Ao}) \times S(A))}{S(Cl)}\right), \quad (1)$$

where $S(A)$ are the absorption cross sections of nuclei A for thermal neutrons (except chlorine), nA are their concentrations, nAo are their base concentrations in average regolith composition used for the modeling, S(Cl) is the absorption cross section of chlorine nuclei, and n_{Cl} is the chlorine concentration. If the value of n_{equ} will be estimated from the modeling of DAN data, the relationship (equation (1)) provides the observational requirement for the content of all other neutron absorbers. To simulate by numerical modeling the variability of chlorine and other neutron absorbers, we admit the variations of chlorine concentration from 0.5 to 1.75 wt % in numerical modeling.

The regolith density was a free parameter during initial modeling, where it was allowed to vary from 1.2 to 2.5 g/cm^3. It was found that a regolith density of 1.8 g/cm^3 is a good approximation of the average regolith density at the first ~60 locations, where DAN active measurements were performed [*Mitrofanov et al.*, 2013b]. Accordingly, the density of the regolith has been fixed at 1.8 g/cm^3 to reduce the number of free parameters of the regolith model.

3.2. DAN Depth Sensitivity

It was found that for many purposes, it is necessary to know the maximal sensitivity depth of DAN active observations. We have estimated this limit based on numerical simulations and ground tests. DAN active measurements were modeled for a double layer regolith structure with a dry layer on the top and pure water ice at the bottom. The water ice layer was placed at depths in range 5–300 cm below dry regolith layer with 1.7 wt % of H_2O and density of 1.8 g/cm^3. It was found that the instrument could not detect a presence of water at depths below about 60 cm. Therefore, the water/ice depth of 60 cm could be used as DAN depth sensitivity limit in the analysis of hydrogen/water distribution in the subsurface. The results of numerical simulations have been validated with DAN ground calibrations, where double layered structure of regolith has been modeled with silicon bricks on the top (with ~2.5 wt % of water) and polyethylene as a replacement of water layer located at the bottom at different depths. This method also concluded depth of ~60 cm as a limit of instrument sensitivity.

3.3. Background Subtraction

In addition to neutron pulsing emission from DAN/PNG, there are two other sources of neutrons. They are the neutrons produced with MSL MMRTG and neutrons produced in the Martian subsurface high-energy charge particles of the galactic cosmic rays (GCRs). The GCR flux and correspondingly produced subsurface neutron flux vary in time modulated by solar activity. The MMRTG neutron flux is continuous and almost omnidirectional. The total number of neutrons emitted by the MMRTG is significantly larger than the number of GCR generated neutrons. The GCR and MMRTG neutrons propagate into the detectors after interacting in regolith and/or in the rover structure. These neutrons create a flux, which is constant on the time scale of DAN active measurements at 10 Hz pulsing frequency of the neutron generator and should be removed as a

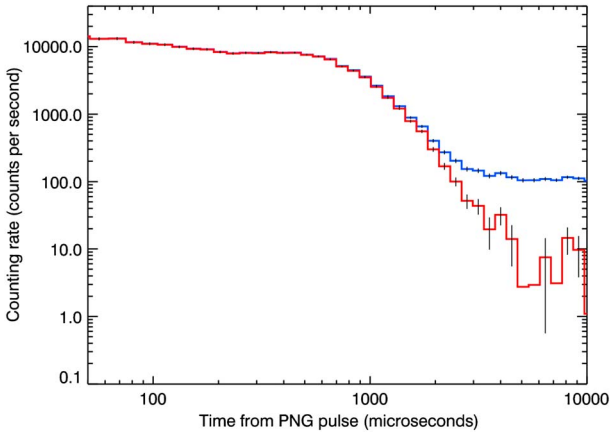

Figure 3. A die-away curve measured by the CTN detector shown before (blue line) and after (red line) background subtraction.

background. The background counting rate $B_{tn,etn}$ (where *tn* and *etn* mean the CTN and CETN detectors here and below) can be estimated separately for DAN detectors using following equation

$$B_{tn,etn} = \frac{\sum_{i=\beta_1}^{\beta_2} N_{tn,etn}(t_i)\cdot\Delta T(t_i)}{\sum_{i=\beta_1}^{\beta_2}\Delta T(t_i)}, \quad (2)$$

where $N_{tn,etn}(t_i)$ is the raw counting rate measured by thermal (*tn*) and epithermal neutron (*etn*) detectors at time bin t_i with a duration $\Delta T(t_i)$ in range of instrument time bins with indexes from β_1 to β_2. The range of instrument time bins selected for the background estimation corresponds to time period 10^4–10^5 μs after a neutron pulse. The procedure $C_{tn,etn}(t_i) = N_{tn,etn}(t_i) - B_{tn,etn}$ removes background and leaves only dynamic albedo of neutrons counting rates (see Figure 3).

3.4. Normalization Procedure

The amplitude of die-away curves measured by CTN and CETN detectors depends on several instrument factors. Thus, the DAN/PNG tritium-rich target is degrading under the bombardment by deuterium ions (during DAN/PNG pulsing) and due to the natural radioactive decay of tritium in the target. Another factor is the aging (due to multiple triggering) of ion source inside DAN/PNG, which may influence on the stability and intensity of neutron output. All these factors lead to the decrease of the neutron pulse intensity with time and corresponding corrections should be included in the data reduction. Figure 4 presents the decrease of DAN/PNG neutron production with surface operational time as measured in the time interval from 10–50 μs after the neutron pulse. Numerical simulations have shown that during this time interval, DAN/DE counting rate does not significantly depend on Martian regolith properties but is dominated by neutrons backscattered inside rover mechanical structures close to the detectors and/or neutron generator. The normalization factor is calculated independently for each DAN active measurement using following equation:

$$M_{tn,etn} = \sum_{i=\gamma_1}^{\gamma_2} C_{tn,etn}(t_i) \quad (3)$$

where $C_{tn,etn}(t_i)$ is the counting rates observed at CTN and CETN detectors at t_i time bin after background subtraction and γ_1 to γ_2 is the instrument time bin indexes corresponding to the time range 10–50 μs after the neutron pulse. The normalized counting rates $A_{th,etn}$ are estimated as

$$A_{tn,etn}(t_i) = \frac{C_{tn,etn}(t_i)}{M_{tn,etn}}. \quad (4)$$

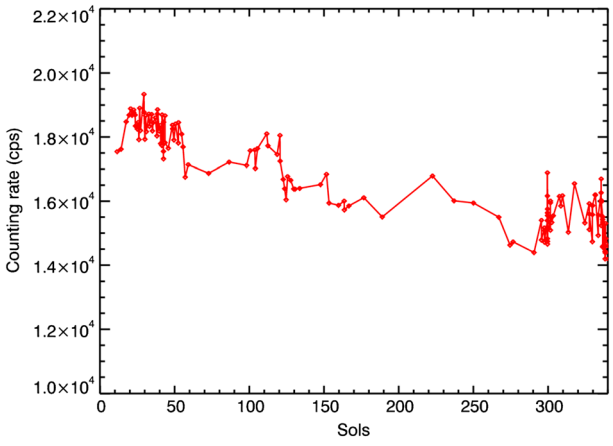

Figure 4. Decrease of DAN/DE counting rate (from start of the MSL surface operations) due to the degradation of DAN/PNG neutron output.

3.5. The Estimation of Regolith Parameters

The main goal of the numerical modeling is to test that the hypothesis that measured the DAN die-away curves can be produced by a given distribution of hydrogen/water in the Martian regolith. The best fit hydrogen concentration, its depth distribution, and other regolith properties could be derived from such test. To enhance sensitivity of this method, it is important to define the optimal time intervals for the comparison between modeled and

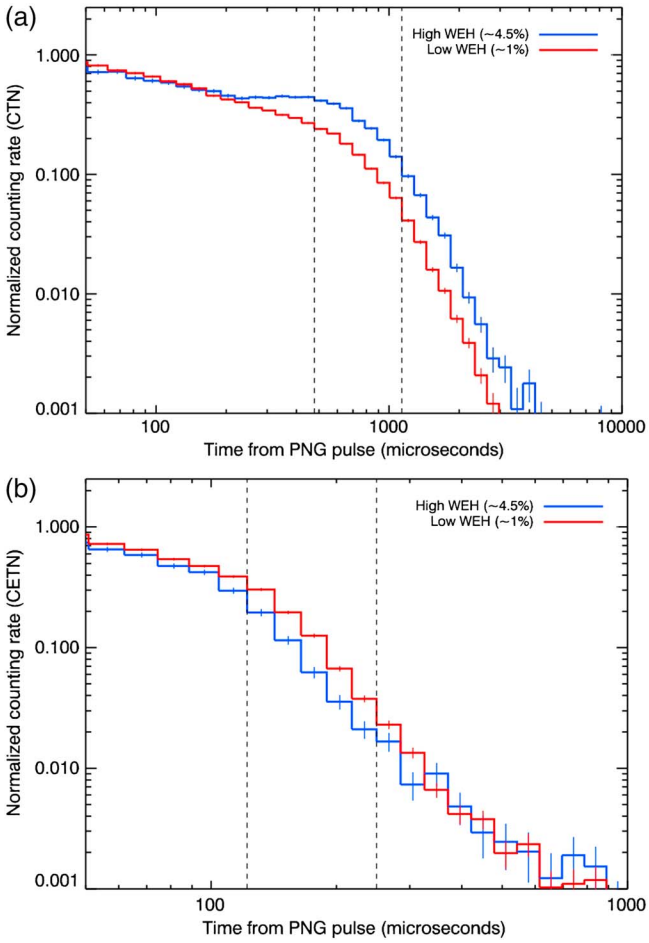

Figure 5. Examples of die-away curves measured by (a) CTN and (b) CETN at H-poor and H-rich sites along MSL traverse. The time intervals selected for the analysis of water abundance are shown by dashed vertical lines.

measured die-away curves. The earliest time bins of die-away curves are mostly populated with the neutrons scattered only in the rover body and do not bring much information about the subsurface properties under the rover. In the later time bins, we observe fewer counts due to the smaller number of neutrons that arrive at the DAN detectors from remote vicinity around the rover position. At such distances, subsurface properties could be significantly different from the footprint right under the rover. The middle time bins show best counting statistic and are mostly populated with neutrons thermalized in the subsurface under the rover. In order to select these optimal time bins and increase sensitivity to hydrogen distribution, we have compared different DAN measurements. According to DAN observations, it is clearly seen that most dry subsurface is observed at Rocknest area, while most hydrogen-rich areas are discovered at Yellowknife Bay (see for example Figure 5). These observations are indirectly supported with sampling analysis accomplished both at the Rocknest dunes and the Yellowknife mudstones, which discovered the presence of hydrated minerals at Yellowknife [see, for example, *Grotzinger et al.*, 2013; *Ming et al.*, 2013]. In our analysis, we have determined time bins showing most contrast between these measurements. Thus, we have selected time interval 478–1135 μs for the thermal neutron detector CTN and time interval 122–249 μs for the epithermal neutron detector CETN (see illustration at Figure 5).

To estimate the regolith model parameters at a particular rover location, a comparison of measurements and numerical model predictions has been accomplished. It was based on the Pearson χ^2 statistical criterion that measured die-away curves are consistent with numerical model predictions for a regolith with given hydrogen water-equivalent (WEH) distribution and chlorine-equivalent concentration ξ_{Cl}, see equation (5).

$$S = \sum_{i=\varepsilon_1^{tn}}^{\varepsilon_2^{tn}} \frac{(A_{tn}(t_i) - W_{tn}(t_i))^2}{(\sigma_{tn}(t_i))^2 + (\omega_{tn}(t_i))^2} + \sum_{k=\varepsilon_1^{etn}}^{\varepsilon_2^{etn}} \frac{(A_{etn}(t_k) - W_{etn}(t_k))^2}{(\sigma_{etn}(t_k))^2 + (\omega_{etn}(t_k))^2}, \quad (5)$$

where $A_{tn,etn}(t_i)$ and $\sigma_{tn,etn}(t_i)$ are the normalized measured count rates (see relationship (4)) and statistical uncertainty of the measurement at time bin t_i of a CTN and CETN die-away curves; $W_{tn,etn}(t_i)$ and $\omega_{tn,etn}(t_i)$ are the count rates and uncertainty (produced in MCNPX Monte Carlo simulation process) at the same bin t_i predicted by a numerical modeling for selected regolith parameters; and ε_2^{etn}, ε_1^{etn}, ε_2^{tn}, ε_1^{tn} are the time bins indexes corresponding to the optimal time intervals for each detector. We have used numerical library with different regolith models to select value S_{min} showing minimal discrepancy between data and model predictions. If selected regolith parameters fit the measurements within given statistical uncertainties the S_{min} value should belong to χ^2_{DOF} distribution with degrees of freedom equal to DOF $= \left(\varepsilon_2^{tn} - \varepsilon_1^{tn}\right) + \left(\varepsilon_2^{etn} - \varepsilon_1^{etn}\right) - \lambda$. The λ here is a number of free parameters of the selected regolith model. In this method, it is necessary to

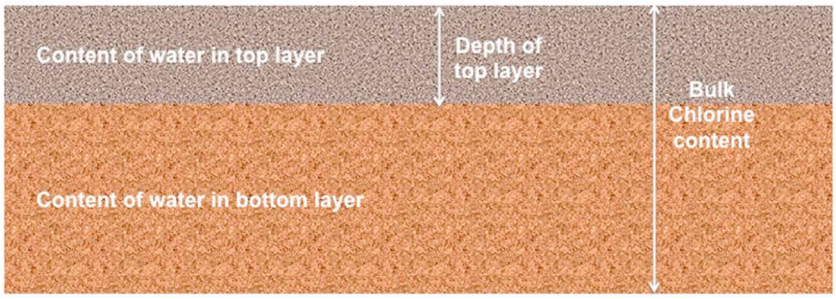

Figure 6. Illustration of two-layer subsurface model selected for DAN data analysis.

postulate confidence probability α and find critical value of $S_{\min}$ when tested hypothesis with given parameters should be rejected. The confidence probability α calculated as

$$\alpha = \int_{\chi^2_{\mathrm{DOF}}(\alpha)}^{\infty} f\left(\chi^2\right) d\chi^2, \tag{6}$$

where $f(\chi^2)$ is the probability density of the χ^2 distribution. Usually the confidence probability level $\alpha = 1\%$ is selected. It means that the given regolith model shall be rejected if $S_{\min} > \chi^2_{\mathrm{DOF}}(0.01)$.

3.6. Estimation of Uncertainties of Model Parameters

The estimation of the model parameter uncertainties is based on a Monte Carlo simulation. Standard recommendations for this approach could be found in various descriptions of numerical methods [see, for example, *Press et al.*, 2007, section 15.6]. The suggested method required multiple Monte Carlo simulations of the measured die-away curves $A^{\mathrm{sim}}_{tn,etn}(t_i)$ according to the statistical uncertainties of measurements $\sigma_{tn,etn}(t_i)$. Then the simulated data have been subjected to the standard process of the regolith parameter estimation described above. In our case, we have repeated this simulation 256 times to get the appropriate distributions of the best fit parameters and use a standard deviation of the sample created for each parameter to take it as the parameter uncertainty.

3.7. Model Selection

Mitrofanov et al. [2013b] have analyzed a set of different models of regolith, starting with homogeneous models and concluding with double-layered models. For these models, the water depth distribution, average content of water, chlorine abundance, and density were considered and studied as free parameters. The first analyses of DAN active data have shown that the average content of water measured during surface operations was 2%, the average content of chlorine was 1.1%, and the average density was estimated as high as 1.8 g/cm^3 [*Mitrofanov et al.*, 2013a]. This analysis has also revealed that there are significant regional variations in water distribution and chlorine-equivalent abundance along Curiosity's traverse. In our analysis, we have used the two-layer model proposed by *Mitrofanov et al.* [2013b]. It includes the variable amounts of hydrogen in the upper and lower layers, variable upper layer thickness, and variable chlorine content (homogenously distributed as a function of depth, see illustration on Figure 6). We find that 99% of rover stops (where DAN active data were acquired) are well fitted with this model [*Mitrofanov et al.*, 2013b].

4. The Description of the DAN Observation Campaign in Yellowknife Bay Area

The Yellowknife Bay formation is a topographic low point bounded by exposed, stratified bedrock which consists of four members named Shaler, Point Lake, Gillespie Lake, and Sheepbed. The highest member of this stratigraphy, Shaler, is found at the intersection of three units observed in orbital images: The hummocky plains, the bedded fractured unit, and a heavily cratered surface [see, for example, *Grotzinger et al.*, 2013]. The topographically lowest members, Gillespie Lake and Sheepbed, consist of well-exposed, apparently resistant lithologies that are more continuous than Shaler and Point Lake. The Gillespie Lake member consists of decimeter-thick beds of uniformly smooth weathering sandstone, whereas Sheepbed consists of fine-grained sedimentary rock suggested to be fluvio-lacustrine siltstones/mudstones cut by light-toned veins [*Grotzinger et al.*, 2013; *Vaniman et al.*, 2013]. The majority of Curiosity's observations in the Yellowknife Bay formation (including drilling and sampling activities) were completed at the Sheepbed member.

It was found that the elemental composition of the Sheepbed is similar to the average Martian upper crust [*McLennan et al.*, 2013]. The APXS and ChemCam instruments detected the presence of Ca and S in rock veins cutting this member, leading to the interpretation that the veins are filled with Ca-sulfates [*McLennan et al.*, 2013]. This interpretation was supported by Mastcam near-IR observations, which are sensitive to the presence of some hydrated minerals [*Bell et al.*, 2013; *Rice et al.*, 2010; *Rice and Bell*, 2011].

The first drilling operations were also done at Sheepbed at sites named as John Klein and Cumberland [*Ming et al.*, 2013]. The drilled samples were analyzed by Chemistry and Mineralogy (CheMin) X-ray diffraction (XRD) and X-ray fluorescence instrument [*Blake et al.*, 2012] and the Sample Analysis at Mars quadrupole mass spectrometer/gas chromatograph/tunable laser spectrometer suite of instruments [*Mahaffy et al.*, 2012].

The sampling operations were also supported by multiband observation with Curiosity's cameras [*Malin et al.*, 2010] and remote elemental composition analysis provided by laser-induced breakdown spectroscopy (ChemCam instrument) [*Wiens et al.*, 2012] and the Alpha-Particle X-ray Spectrometer (APXS instrument) [*Campbell et al.*, 2012].

The CheMin data have revealed a significant amount of clays in the drill samples. At both the John Klein and Cumberland drilling sites, ChemMin XRD data indicate a ~20% wt abundance of phyllosilicates [see *Vaniman et al.*, 2013]. It is thought that these phyllosilicates were formed in an aqueous environment, possibly involving two or more episodes of water moving through the Yellowknife Bay members [*Grotzinger et al.*, 2013; *Vaniman et al.*, 2013].

The joint multi-instrument analysis has shown that the aqueous environment in Sheepbed can be characterized as being lacustrine, neutral in pH, and low in salinity. Variable redox states of both iron and sulfur species are found, and the presence of the key biogenic elements C, H, O, S, and P is indicated [*Grotzinger et al.*, 2013; *Mclennan et al.*, 2013; *Ming et al.*, 2013; *Vaniman et al.*, 2013]. It has been concluded that during the late Noachian/earlier Amazonian periods, this area constituted a habitability environment [*Grotzinger et al.*, 2013].

Up to sol 295, DAN has made 12 measurements of the Sheepbed member and detected distinctive local variations of water and chlorine content within it ([*Mitrofanov et al.*, 2013b] odometry 640–727 m). In some cases, these variations may correlate with geological context.

Based on the observed diversity, a special set of observations was acquired, named the "DAN campaign." The purpose of this campaign was to determine whether DAN-determined variations in hydrogen/chlorine bulk composition were correlated with easily observed geological context (exposed strata) using measurement intervals comparable in scale to the horizontal sensing "footprint" of DAN. The DAN footprint is estimated as a circle area with a radius of about 1.5 m, centered at the backside of the rover, and equidistant between the DAN/PNG and DAN/DE components. Based on these assumptions, Curiosity was commanded to make DAN 18 active measurements every 0.75–1 m along the ~15 m traverse (odometry 751–765 m) to provide oversampling of the DAN footprint between successive measurements.

The Sheepbed and Gillespie Lake are the most continuous members of the Yellowknife Bay formation. The contact between these units is expressed at the surface as a distinct, step-like boundary with a height of about 40 cm. Several options for the drive were considered to take into account science requests to cross several boundaries between different geological units (including primary contact between Sheepbed and Gillespie Lake), long-term planning tasks (i.e., placing the rover in a desirable location for other objectives at the end of the traverse), and rover mechanical limitations related to climbing and wheel slippage (there is a restriction against rover tilt angles ≥15°). At each stop along traverse route, DAN made high signal-to-noise measurement in its active mode, with a duration of 15 min at 10 Hz (i.e., 9000 emitted neutron pulses per stop). The area of the Curiosity/DAN traverse (for sol 299 which is the major part of the traverse) is presented in Figure 7. This figure shows the DAN footprints for each observation and three boundaries separating the geological subunits inside the Sheepbed and Gillespie Lake, extending roughly perpendicular to the rover traverse. It includes two secondary boundaries between subunits inside the Sheepbed and Gillespie Lake and one primary contact area between the Sheepbed and Gillespie Lake members. Their more detailed description is presented below.

The boundary #1 (see Figure 7) is located inside the Sheepbed and separates the upper and lower subunits of the clay-rich Sheepbed unit.

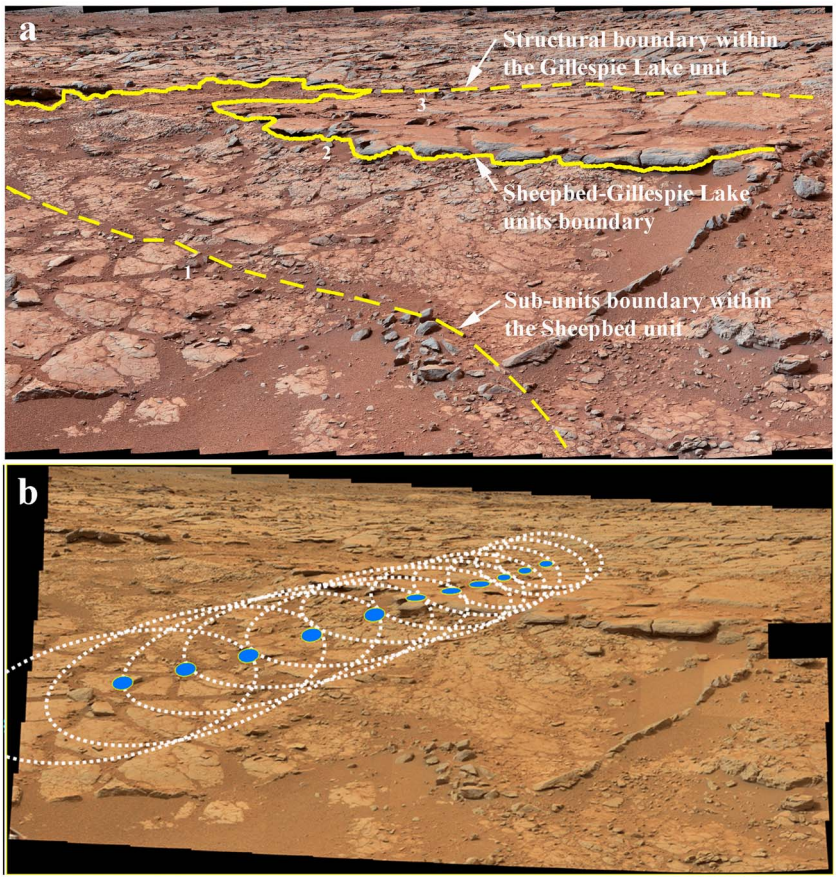

Figure 7. (a) Mastcam mosaic of the Yellowknife Bay formation. Boundaries between different subunits inside Sheepbed and Gillespie are shown in white. The middle one corresponds to the primary Sheepbed/Gillespie contact. (b) Major part of the DAN campaign (sol 299, stops #4–14, shown by blue). The white dashed lines show the DAN footprints for each observation.

The boundary #2 (see Figure 7) is the primary contact between the Sheepbed and Gillespie Lake units.

The boundary #3 (see Figure 7) is located inside the Gillespie Lake and delineates a distinctive structural heterogeneity inside the Gillespie Lake unit, in the form of a linear, shallow trough filled with debris of from unit fragmentation mixed with loose material.

These boundaries distinguish four different subunits: Sheepbed subunit #1 (area prior boundary #1), Sheepbed subunit #2 (area between boundary #1 and boundary #2), Gillespie Lake subunit #1 (area between boundary #2 and boundary #3) and Gillespie Lake subunit #2 (area past boundary #3).

The DAN campaign began with two measurements of the drilling sites, and then the traverse continued across the Sheepbed/Gillespie Lake contact area.

5. DAN Measurements Along Sheepbed/Gillespie Lake Traverse

The DAN campaign was initiated after drilling and sample analysis operations at the Cumberland site. On sol 295, Curiosity executed 180° turn in place to make DAN high signal-to-noise ratio (SNR) measurements with the instrument directly above the John Klein and then Cumberland drilling sites. *Mitrofanov et al.* [2013b] has shown that drilling sites can be characterized with two-layer model with 1.1–1.4% of WEH in the top layer with thickness ~20 cm, 2.6–3.0% of WEH at the bottom layer, and chlorine-equivalent abundance ranged within 0.8–1.1%. It relatively well corresponds to the results of sampling analysis [*Ming et al.*, 2013; *Vaniman et al.*, 2013].

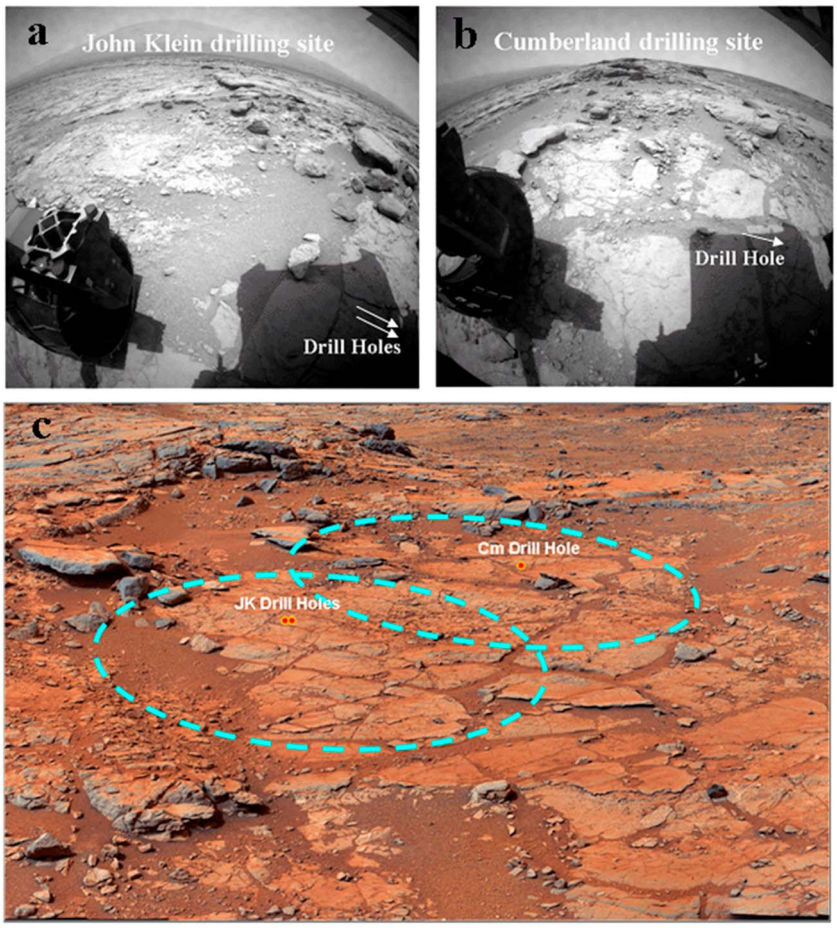

Figure 8. (a) RHazCam image of the DAN footprint area taken at the John Klein drilling area. The borehole of John Klein is shown by arrows. (b) RHazCam image of the DAN footprint area taken at the Cumberland drilling area. The borehole of Cumberland is shown by an arrow. (c) Mastcam mosaic of the Yellowknife Bay formation showing the DAN footprints for the observations of the drilling sites.

All the DAN measurements during the campaign have been documented with images acquired by the Curiosity Rear Hazard Cameras (RHazCam) [see *Maki et al.*, 2012]. For example, Figure 8 show two photos taken from the RHazCam, which document the position of Curiosity's aft end, with the DAN instrument above the drill holes at John Klein and Cumberland.

On sol 297, Curiosity drove from the drilling area to a start point for the DAN traverse and made the first three stops with DAN active measurements commanded at 1 m intervals. Camera images obtained at these stops were used to assess navigation over this initial part of the traverse and take into account corrections (e.g., due to wheel slippage) for the remainder of the DAN traverse. The primary part of the DAN traverse started on sol 299, 5 m away from the Sheeped/Gillespie Lake contact (boundary #2) and 1.5 m away from the boundary #1 between the clay-bearing Sheepbed upper (Selwyn section) and lower subunits (see Figure 7). On sol 299, Curiosity made 11 stops along the traverse (see Figure 7), all of them with high SNR DAN active measurements supported by RHazCam images for documentation. During this traverse, rover crossed the boundary #2 (Sheepbed/Gillespie Lake contact, see Figure 7). The last stop in this sequence was completed at the top of the Gillespie Lake member, near the boundary #3 (see Figure 7). During the planning of sol 301, it was found that rover resources were available to continue the DAN traverse. Four additional stops were made, separated by 0.75 m. In total, the DAN campaign with short-interval measurements lasted for 5 sols. It was completed at the end of sol 301 and included 18 separate stops.

In Figure 9, we present two profiles of epithermal and thermal neutron fluxes measured by DAN in active mode for the different rover stops along the traverse. The variations of epithermal neutron flux are most

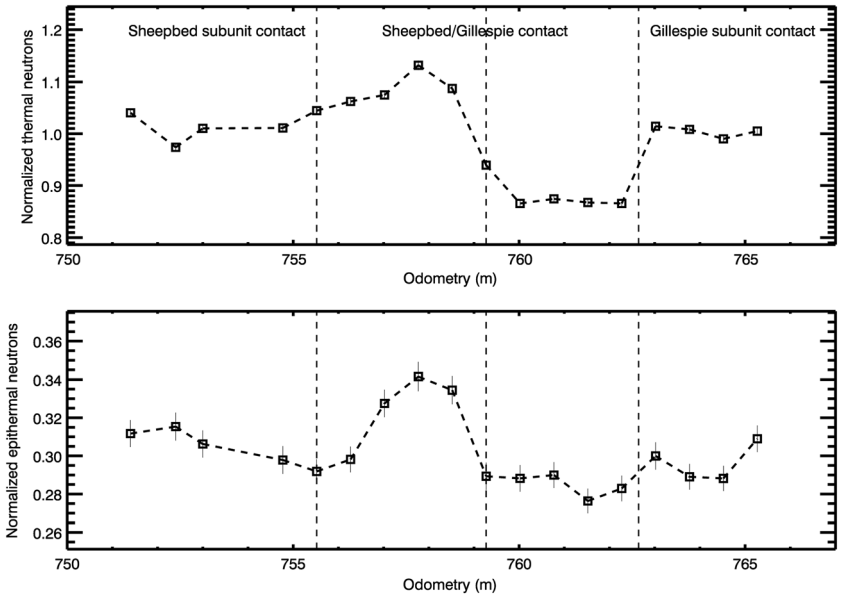

Figure 9. (top) Profile of the thermal neutron flux measured by DAN/DE in active mode along the Curiosity traverse during the DAN campaign (sols 297–301). (bottom) Profile of the epithermal neutron flux measured by DAN/DE in active mode along the Curiosity traverse during the DAN campaign (sols 297–301).

sensitive to the variation of subsurface hydrogen content, while the variations of thermal flux may be caused by both variations in hydrogen and the presence of neutron absorbing elements. The most prominent and significant feature on both plots is the rise of the neutron flux between stops #5 and #10. In statistical terms, the significance of the difference between these stops corresponds to more than 20σ for the thermal neutrons and more than 5σ for the epithermal neutrons. In both cases, the probability that observed effect has arisen due to random fluctuations is negligible. Another one statistically significant variation of thermal neutron flux is found between stops #14 and #15. The revealed differences correlate well with the previously mapped geologic boundaries presented in Figure 7. They are shown on Figure 9 by dashed lines. The most significant effect is related with boundary #2 (Sheepbed/Gillespie Lake contact area). The observed variations of thermal and epithermal neutrons may indicate both changes of average content of water and the abundance of thermal neutron-absorbing elements.

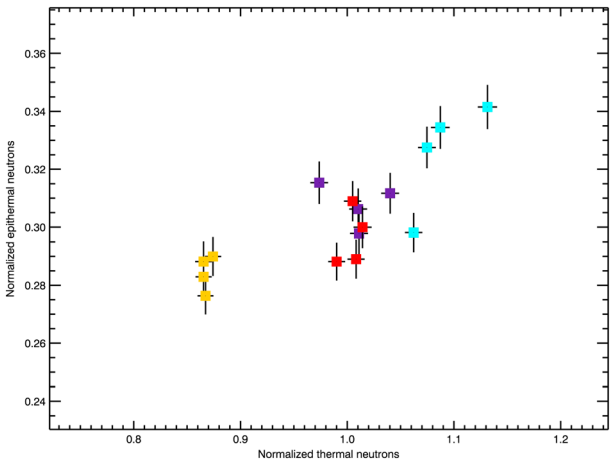

Figure 10. Scatterplot showing the correlation between thermal and epithermal neutron fluxes measured in active mode during the DAN campaign. The measurements are combined in geologic context groups shown by different colors: violet for the Sheepbed subunit #1, cyan for the Sheepbed subunit #2, yellow for the Gillespie Lake subunit #1, and finally red for the Gillespie Lake subunit #2.

In Figure 10, we present a scatterplot showing the correlation between the thermal and epithermal neutron fluxes measured in active mode at different stops during DAN campaign. The dots on this plot are specially shown with different color in accordance with previously mapped geologic context. The whole traverse may be split into four subunits located between boundaries #1 and #3 (see also definition in section 4). Violet is used for the first Sheepbed subunit #1 (before boundary #1), cyan for the upper Sheepbed subunit #2 (between boundary #1 and boundary #2), yellow for the lower subunit #1 at

Table 1. DAN Model Parameters of Regolith for Different Sheepbed and Gillespie Lake Members of Yellowknife Bay Formation

Name	Start (m)	Stop (m)	Top Water (%)	Depth (cm)	Bottom Water (%)	Chlorine (%)	Average Water Within 60 cm (%)	Comments
Sheepbed subunit #1	751.4	754.8	1.40 ± 0.14	20 ± 3	2.9 ± 0.3	1.05 ± 0.07	2.40 ± 0.17	Group#1: Probability to accept two-layer model is equal to 53%.
Sheepbed subunit #2	756.27	757.8	1.50 ± 0.12	30 ± 5	2.8 ± 0.3	0.80 ± 0.05	2.15 ± 0.15	Group#2: Probability to accept two-layer model is equal to 68%.
Gillespie Lake subunit #1	760.02	762.3	1.70 ± 0.16	20 ± 4	2.9 ± 0.4	1.5 ± 0.1	2.50 ± 0.19	Group#3: Probability to accept two-layer model is equal to 91%.
Gillespie Lake subunit #2	763.02	765.3	1.4 ± 0.3	10 ± 7	2.4 ± 0.3	1.3 ± 0.1	2.23 ± 0.14	Group#4: Probability to accept two-layer model is equal to 15%.

the Gillespie Lake unit before the lineal shallow trough that cuts the unit (between boundaries #2 and #3), and finally, red for the upper Gillespie Lake subunit #2, after the trough (past boundary #3). It is seen that the distribution of points in Figure 10 is not random and some of them are combined in groups by color (geologic context). This association supports the suggestion that there is some correlation between geologic context derived from the visual observations (both from rover cameras and from high-resolution orbital images) of the overlaying surface and DAN measurements. The most significant difference is observed between Sheepbed upper subunit #2 (cyan symbols) and Gillespie Lake subunit #1 (yellow symbols). They are two successive subunits separated by the contact area between Sheepbed and Gillespie Lake. This corresponds well with the variations in neutron fluxes along traverse, which we have presented and discussed in Figure 9. Qualitatively, one may say that Gillespie Lake subunit #1 has more water, because epithermal neutron flux decreased when rover moved from Sheepbed upper subunit #2 to Gillespie Lake subunit #1. We also may expect a significantly higher abundance of neutron-absorbing elements at the Gillespie Lake subunit #1, because thermal neutron flux also significantly decreases (instead of the increasing as one could expect in case of only water content variation).

We have compared each DAN observation during traverse with a two-layer model of the subsurface (see Figure 6), with a variable distribution of water and variable content of chlorine (the same type of model as was applied to the previous observations).

In Table 1 and Figure 11, several profiles of best fit model parameters are shown which have been averaged for the different DAN measurements within the Sheepbed and Gillespie Lake subunits and subunit contacts. They include variations of the upper layer water abundance, bottom layer water abundance, depth of the interface between the layers, bulk equivalent chlorine abundance, and bulk water abundance (estimated within 60 cm depth).

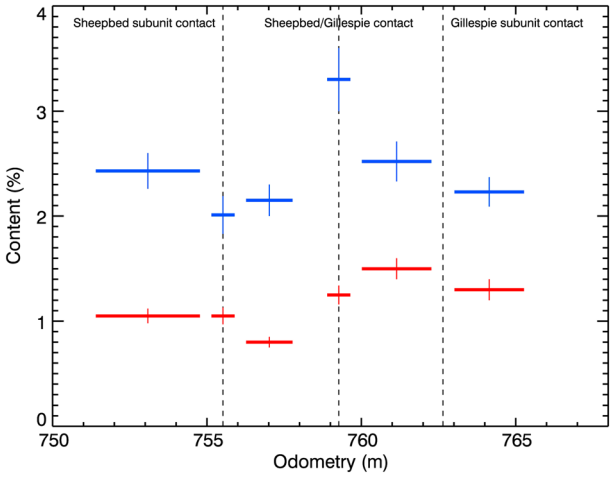

Figure 11. Profiles of the average water-equivalent hydrogen (blue) and chlorine-equivalent neutron absorption (red) within 60 cm depth. All the profiles are averaged for different subunits (including measurements for boundaries #1 and #2) along Curiosity traverse during the DAN campaign (see Table 2). The boundaries #1–#3 are shown by dashed lines.

Stops #1–4 are at the beginning of the DAN traverse. The analysis of these measurements has revealed that bulk water distribution does not significantly change among them, and it is similar to the distribution observed at the drilling sites. We combined stops #1–4 in one group because they belong to the same subunit (Sheepbed subunit #1, prior boundary #1) and could be fitted with one subsurface model (probability to fit these measurements as one ensemble is more than 50%, see Table 1). The top water abundance is 1.40 ± 0.14%, and the depth to the bottom layer is 20 ± 3 cm. The water abundance in the bottom layer is 2.9 ± 0.3%, and the

average chlorine abundance is 1.05 ± 0.07%. The bulk water content in the 60 cm of subsurface is estimated to be 2.40 ± 0.17% WEH (see Table 1).

At stop #5, Curiosity crossed an area of loose soil corresponding to the boundary #1 between the upper and lower subunits 1 and 2 inside the Sheepbed. Modeling of the DAN data shows that it contains less WEH (about 1%) at the very top of the subsurface, in comparison with the previous stops (#1–4), where fractured rock outcrops are dominant in the DAN footprint. But the thickness of this layer is very thin at ~5 cm. A plausible interpretation of these results is that the water distribution at this spot is close to homogeneous. It could be characterized just by one parameter such as the average content of water in a single-layer model. This content is estimated to be about 2.0 ± 0.2 wt %.

Stops #6–9 are combined in the second group. They are located on eroded, fractured outcrops between boundary #1 and boundary #2 and belong to the Sheepbed subunit #2. According to the best fit model estimations (these measurements are fitted as one group with probability equal to 68%), the upper layer at stops #6–9 contains about 1.50 ± 0.12% WEH, with an upper layer thickness of 30 ± 5 cm. This is deeper than the best fit model of the subsurface found at stops #1–4. At the bottom of this layer, the regolith is enriched with ~2.8 ± 0.3% WEH. The net effect is a difference in bulk water abundances with 2.40 ± 0.17% WEH at stops #1–4 and 2.15 ± 0.15% WEH at stops #6–9. The best fit chlorine-equivalent abundance also displays a relatively prominent difference between the first (stops #1–4) and the second part (stops #6–9) of the DAN traverse within the Sheepbed member. It smoothly drops from the values of 1.05 ± 0.07% at the beginning of the DAN traverse to ~0.80 ± 0.05% (see also Table 1).

Stop #10 is an intermediate stop, which could be addressed to boundary #2. It corresponds to the crossing through the contact area between Sheepbed and Gillespie Lake. It is described by the following parameters: upper layer water abundance is 1.20 ± 0.17%, thickness of the upper layer is about 20 ± 3 cm, water abundance in the lower layer is 4.4 ± 0.5%, and chlorine abundance −1.25 ± 0.10%. It is significantly different from the previous group, especially by the higher abundance of equivalent chlorine and WEH in the lower layer.

Stops #11–18 are the locations on the surface where the DAN signal was collected from the Gillespie Lake member. They may be divided into two parts: #11–14 (third group, Gillespie Lake subunit #1) and #15–18 (fourth group, Gillespie Lake subunit #2), separated by the boundary #3, linear shallow trough cutting the Gillespie Lake.

In the case of third group (the measurements included in this group are fitted with probability equal to 91%), the major difference with previous groups is a significant increase in chlorine-equivalent abundance from 0.80 ± 0.05% (second group) up to 1.5 ± 0.1%. The water distribution at the first stops on the Gillespie Lake member can be characterized with ~1.70 ± 0.16% of H_2O, the upper layer down to a depth of about 20 ± 4 cm, where it changes to 2.9 ± 0.4%. The best fit bulk water content is 2.5 ± 0.2%.

Stops #15–18 are combined into fourth group as belonged to Gillespie Lake subunit #2 (they are fitted together with probability equal to 15%). They are also enriched in chlorine up to 1.3 ± 0.1%, but water distribution is significantly changed to ~1.4 ± 0.3% of H_2O in the upper layer, with a depth of only about 10 ± 7 cm and ~2.4 ± 0.3% of H_2O in the lower layer. Here more water is available close to the surface level, but bulk water (within 60 cm) is similar to second group (see Table 1 and Figure 11) and equal to 2.23 ± 0.14%.

6. Conclusions

The DAN campaign was the first attempt to use the targeted DAN observations and to search for possible correlations between the DAN measurements of bulk composition of water and chlorine with independently assessed geologic context on a local scale. It was based on the special selection of the rover's route through the visually distinguished different geologic subunits and contact areas between them.

It was revealed that thermal and epithermal neutron fluxes measured in the DAN active mode have statistically significant variations along the traverse. These variations correlate well with contacts between different subunits. The largest difference is observed at the contact between the two members of the Yellowknife Bay formation: Sheepbed and Gillespie Lake. Other distinguished subunits also show inhomogeneity of neutron flux from the subsurface. They can be characterized by both different absolute

values of neutron flux and different ratio between the measured fluxes of epithermal and thermal neutrons. This indicates that the distribution of hydrogen-rich materials and neutron-absorbing elements is nonhomogeneous on the small scale (<20 m) traversed by the rover during the DAN observational campaign.

In our analysis, we have divided the DAN measurements into four groups in accordance with geologic context (Sheepbed subunits #1 and 2 and Gillespie Lake subunits #1 and 2, see Table 1) and supported them with the estimations of WEH and chlorine-equivalent subsurface distributions. To make such estimations, we have used a two-layer model with a variable distribution of water as a function of depth and variable content of chlorine. The implementation of this model has revealed that both water and chlorine vary along the traverse, showing some correlations with the traversed subunits. The variations in both average water and average chlorine between different groups are significant. The probability of explaining these variations (presented on Figure 11) as statistical noise around a constant value is negligible (below 0.1% according Pearson chi-square test criterion). This means that the difference found corresponds to more than 3σ of statistical significance.

The bulk abundance of water measured within 60 cm below surface changes from 2.15 ± 0.15% at the subunit #2 inside Sheepbed (right before Sheepbed/Gillespie Lake contact boundary area, boundary #2 on Figure 7) up to 2.5 ± 0.2% at the beginning of the Gillespie Lake subunit #1 (afterward boundary #2 on Figure 7). The variations of neutron absorption elements measured as chlorine-equivalent concentration are even higher. For the same subunits, it changes from 0.80 ± 0.05% (inside Sheepbed) up to 1.5 ± 0.1% on the top of Gillespie Lake.

The distribution of water as a function of depth also slightly changes for different subunits. The water abundance in the upper subsurface layer is approximately the same, showing nonsignificant variations within 1.4–1.7% for all the four subunits (see Table 1). But the thickness of the upper layer may change from 10 cm (Gillespie Lake subunit #2) down to 30 cm (Sheepbed subunit #2). The water content in the lower layer ranges between 2.4% and 2.9% for different subunits. The primary contact area (boundary #2) between the Sheepbed and Gillespie Lake members is the most hydrogen-rich area (average water >3%), is significantly nonhomogeneous (~1% in the upper layer and ~4% in the lower layer), and characterized with an intermediate content of equivalent chlorine (~1.25%)

DAN has a large footprint area with a radius of about 1.5 m under the aft end of the rover. It is significantly larger than the footprint of the contact and remote measurements of elemental composition provided by the other science instruments onboard Curiosity. DAN provides a unique capability to look below the surface as deep as 60 cm and study the depth distribution of water and neutron-absorbing elements. Thus, DAN measurements are complementary to other Curiosity observations. A good example of this is the observation of the Curiosity's drilling sites in the Sheepbed mudstones, which were completed as a part of the DAN observation campaign. The drilling holes themselves are much smaller than the DAN footprint, but DAN measures neutron flux originated at larger depths than was achieved during the drilling operations. The comparison between DAN average bulk composition of water and chlorine with "pinpoint" sampling and contact measurements suggests that there is compositional heterogeneity in the Sheepbed member at a scale of tens of cubic centimeter.

Acknowledgments

The DAN team is thankful to the highly professional MSL project team members, who have maximized opportunities for DAN measurements on Mars. We would like to express our special thanks to the Rover Planner Team, MSL engineers, and scientists who made these DAN measurements real. The DAN team very much appreciates the work of colleagues from the N. L. Dukhov Institute for Automatics for the development of the reliable PNG for this experiment. Also, the DAN team appreciates the valuable cooperative support of the two national space agencies, Roscosmos and NASA, which, working together, have made this Russian-contributed instrument possible on an American rover. Finally, the team thanks the Curiosity science community, which provided essential comments and advice to the DAN team during numerous discussions.

References

Anderson, R. C., et al. (2012), Collecting samples in Gale Crater; an overview of the Mars Science Laboratory sample acquisition, sample handling and processing system, *Space Sci. Rev.*, *170*, 57–75, doi:10.1007/s11214-012-9898-9.

Bell, J. F. (2008), *The Martian Surface. Composition, Mineralogy and Physical Properties*, Cambridge Univ. Press, Cambridge, U. K., ISBN-13 978-0-521-86698-9.

Bell, J. F. III, et al. (2013), Initial Multispectral Imaging Results from the Mars Science Laboratory Mastcam Investigation at the Gale Crater Field Site. Lunar Planet. Sci. Conf. 44, abst. #1417.

Berger, J. A., M. E. Schmidt, R. Gellert, and P. L. King (2014), Comparing Gale crater and Gusev crater enrichments of fluid-mobile elements measured by alpha-particle X-ray spectrometers on Mars, Lunar Planet. Sci. Conf. 45, abst. #2285.

Bibring, J. P., et al. (2006), Global mineralogical and aqueous Mars history derived from OMEGA/Mars Express data, *Science*, *312*, 400–404.

Bish, D. L., et al. (2013), X-ray Diffraction Results from Mars Science Laboratory: Mineralogy of Rocknest at Gale Crater, *Science*, *341*, doi:10.1126/science.1238932.

Blake, D. F., et al. (2012), Characterization and Calibration of the CheMin Mineralogical Instrument on Mars Science Laboratory, *Space Sci. Rev.*, *170*, 341–399, doi:10.1007/s11214-012-9905-1.

Blake, D., et al. (2013), Curiosity at Gale Crater, Mars: Characterization and Analysis of the Rocknest Sand Shadow, *Science*, *341*, doi:10.1126/science.1239505.

Campbell, J. L., G. M. Perret, R. Gellert, S. M. Andrushenko, N. L. Boyd, J. A. Maxwell, P. L. King, and C. D. M. Schofield (2012), Calibration of the Mars Science Laboratory alpha particle X-ray spectrometer, *Space Sci. Rev.*, *170*, 319–340, doi:10.1007/s11214-012-9873-5.
Crane, T. W., and M. P. Baker, (1991), Neutron Detectors, in *Passive Nondestructive Assay of Nuclear materials*, edited by D. Reilly, N. Ensslin, adn H. Smith Jr., Nuclear Regulatory Commission, NUREG/CR-5550, March 1991, p. 379.
Gellert, R., et al. (2014), APXS measurements along the MSL traverse at Gale crater, Mars, Lunar Planet. Sci. Conf. 45, abst. #1876.
Golombek, M., et al. (2012), Selection of the Mars Science Laboratory Landing Site, *Space Sci. Rev.*, *170*, 641–737.
Grotzinger, J. P. (2009), Beyond water on Mars, *Nat. Geosci.*, *2*, 2331–233.
Grotzinger, J. P., et al. (2012), Mars Science Laboratory Mission and Science Investigation, *Space Sci. Rev.*, *170*, 5–56, doi:10.1007/s11214-012-9892-2.
Grotzinger, J. P., et al. (2013), A Habitable Fluvio-Lacustrine Environment at Yellowknife Bay, Gale Crater, Mars, *Science*, doi:10.1126/science.1242777.
Hardgrove, C., J. Moersch, and D. Drake (2011), Effects of geochemical composition on neutron die-away measurements: Implications for Mars Science Laboratory's Dynamic Albedo of Neutrons experiment, *Nucl. Instr. Meth. Phys. Res.*, *659*(1), 442–455.
Hardgrove, C., et al. (2013), Chlorine and Hydrogen Contents from the First 90 Sols of MSL DAN Active Measurements, 44th Lunar and Planetary Science Conference, LPI Contribution No. 1719.
Jun, I., et al. (2013a), Neutron Background Environment Measured by the Mars Science Laboratory's (MSL) Dynamic Albedo of Neutrons (DAN) Instrument During the First 100 Sols, 44th Lunar and Planetary Science Conference, LPI Contribution No. 1719, p.1608
Jun, I., et al. (2013b), Neutron background environment measured by the Mars Science Laboratory's Dynamic Albedo of Neutrons instrument during the first 100 sols, *J. Geophys. Res. Planets*, *118*, 2400–2412.
Leshin, L. A., et al. (2013), Curiosity Rover Volatile, Isotope, and Organic Analysis of Martian Fines with the Mars, *Science*, *341*, doi:10.1126/science.1238937.
Litvak, M. L., et al. (2008), The Dynamic Albedo of Neutrons (DAN) Experiment NASA's 2009 Mars Science Laboratory, *Astrobiology*, *8*(3), 605–612.
Litvak, M. L., et al. (2013), Estimation of Natural Neutron Emission from the Surface of the Gale Crater from the Ground Data from DAN and the Orbital Data from HEND 44th Lunar and Planetary Science Conference, LPI Contribution No. 1719, p.1864
Mahaffy, P. R., et al. (2012), The Sample Analysis at Mars investigation and instrument suite, *Space Sci. Rev.*, *170*, 401–478, doi:10.1007/s11214-012-9879-z.
Maki, J., D. Thiessen, A. Pourangi, P. Kobzeff, T. Litwin, L. Scherr, S. Elliott, A. Dingizian, and M. Maimone (2012), The Mars Science Laboratory Engineering Cameras, *Space Sci. Rev.*, *170*(1–4), 77–93.
Malin, M. C., et al. (2010), The Mars Science Laboratory (MSL) Mast-mounted Cameras (Mastcams) Flight Instruments. Lunar Planet. Sci. Conf. 41, abst. #1123.
Meslin, P., et al. (2013), Soil Diversity and Hydration as Observed by ChemCam at Gale Crater, Mars, *Science*, *341*, doi:10.1126/science.1238670.
McLennan, S. M., et al. (2013), Elemental Geochemistry of Sedimentary Rocks in Yellowknife Bay, Gale Crater, Mars, *Science*, doi:10.1126/science.1244734.
Ming, D. W., et al. (2013), Volatile and Organic Compositions of Sedimentary Rocks in Yellowknife Bay, Gale Crater, Mars, *Science*, doi:10.1126/science.1245267.
Mitrofanov, I. G., et al. (2012), Experiment for measurements of Dynamic Albedo of Neutrons (DAN) onboard NASA's Mars Science Laboratory, *Space Sci. Rev.*, *170*(1–4), 559–582.
Mitrofanov, I. G., et al. (2013a), Studying of water content in Mars' Gale Crater: The first results of the DAN experiment on the NASA Curiosity rover, Doklady Physics, Russian Academy of Sciences, *59*(3), 126–128, doi:10.1134/S1028335814030112.
Mitrofanov, I. G., et al. (2013b), Content of water and chlorine in the Martian soil along the first 1900 meters of the traverse of Curiosity, as measured by DAN instrument onboard the Rover.
Murchie, S. L., et al. (2009), A synthesis of Martian aqueous mineralogy after 1 Mars year of observations from the Mars Reconnaissance Orbiter, *J. Geophys. Res.*, *114*, E00D06, doi:10.1029/2009JE003342.
Pelowitz, D. B. (2011), MCNPX User's Manual, Version 2.7.0, LANL Report LA-CP-11-00438, Los Alamos National Laboratory.
Press W. H., S. A. Teukolsky, W. T. Vetterling, B. P. Flannery (2007), *NUMERICAL RECIPES. The Art of Scientific Computing*, 3rd ed., Cambridge Univ. Press, Cambridge, U. K., ISBN-13 978-0-521-88068-8
Rice, M. S., J. F. Bell, E. A. Cloutis, A. Wang, S. W. Ruff, M. A. Craig, D. T. Bailey, J. R. Johnson, P. A. de Souza, and W. H. Farrand (2010), Silica-rich deposits and hydrated minerals at Gusev Crater, Mars: Vis-NIR spectral characterization and regional mapping, *Icarus*, *205*(2), 375–395.
Rice, M. S., and J. F. Bell III (2011), Mapping Hydrated Materials with MER Pancam and MSL Mastcam: Results from Gusev Crater and Meridiani Planum, and Plans for Gale Crater, Amer. Geophys. Union Fall Mtg., abst. #P22A-02.
Squyres, S. W., J. P. Grotzinger, J. F. Bell III, W. Calvin, and P. R. Christensen (2004), In-situ evidence for an ancient aqueous environment at Meridiani Planum, Mars, *Science*, *306*, 1709–1714.
Squyres, S. W., et al. (2012), Ancient Impact and Aqueous Processes at Endeavour Crater, Mars, *Science*, *336*, 570–576.
Tate, C. G., et al. (2013), Diurnal Variations in MSL DAN Passive Measurements with Atmospheric Pressure and Soil Temperature, 44th Lunar and Planetary Science Conference, LPI Contribution No. 1719, p.1601
Wiens, R. C., et al. (2012), The ChemCam Instrument Suite on the Mars Science Laboratory (MSL) Rover: Body Unit and Combined System Tests, *Space Sci. Rev.*, *170*, 167–227, doi:10.1007/s11214-012-9902-4.
Vaniman, D. T., et al. (2013), Mineralogy of a Mudstone at Yellowknife Bay, Gale Crater, Mars, *Science*, doi:10.1126/science.1243480.